Frequency-Domain Modal Analysis for Power-Electronic-Based Power Systems

Chou, Shih-Feng; Wang, Xiongfei; Blaabjerg, Frede

Published in:
IEEE Transactions on Power Electronics

DOI (link to publication from Publisher):
10.1109/TPEL.2020.3032736

Publication date:
2021

Document Version
Accepted author manuscript, peer reviewed version

This article has been accepted for publication in a future issue of this journal, but has not been fully edited. Content may change prior to final publication. Citation information: DOI 10.1109/TPEL.2020.3032736, IEEE Transactions on Power Electronics

Frequency-Domain Modal Analysis for Power-Electronic-Based Power Systems

Shih-Feng Chou, *Member, IEEE*, Xiongfei Wang, *Senior Member, IEEE*, and Frede Blaabjerg, *Fellow, IEEE*

***Abstract*—This letter presents two frequency-domain modal analysis methods, "peak-picking" and "circle fit" methods, used for current control interactions of grid-connected voltage source converters (VSCs). Differing from the conventional resonance mode analysis, the modal impedances are analyzed with their Nyquist plots, instead of the magnitude-frequency response, which leads to an accurate prediction on the damping behavior of system. Experimental tests verify the theoretical modal analysis methods.**

***Index Terms*—Eigenvalue, impedance model, modal analysis, resonances mode, voltage source converters (VSCs)**

I. Introduction

A rapid increase in the number of renewable resources in the current power systems are seen, where voltage source converters (VSCs) are generally used as interfacing converters. The multi-time scale control dynamics of VSCs bring the challenge to analyzing grid stability [1]. To investigate these dynamics, the impedance-based methods have been widely used in the frequency-domain stability analysis in the power system, where the stability can be determined by a minor feedback loop composed by the ratio of equivalent impedances [2]. However, the impedance-based analysis method merely predicts the stability from the bus of interest, and fails to provide a global view on the system oscillation modes, and on the contributions of VSCs to the oscillation modes [3].

The influences of components to the harmonics in power systems have been quantitatively analyzed with the concept of resonance mode analysis in [4], which concludes that the resonances occur at the singular points in the nodal admittance matrix of the passive network of the system derived from the eigenvalue analysis. Thus, the magnitude-frequency responses of eigenvalues have been studied through sensitivity analysis and quantified indices of passive components, such as participation factors and eigenvalue sensitivities with respect to the components, are given [5]. Then, this resonance mode analysis was later implemented for the converter-based power systems, e.g. in the traction networks [6], micro grids [7], and wind power plants [8]. However, the VSCs were merely considered as the harmonic sources in [8], and the other analyses in [6] and [7] only focus on the magnitude-frequency responses of the eigenvalues, while the phase-frequency responses were overlooked, which are critical to the VSC-based systems [9].

In this letter, two frequency-domain modal analysis methods introduced in [10], which are "peak-picking" method in the magnitude-frequency response and "circle fit" method in the Nyquist plot, are implemented to analyze the resonance modes of VSC-based power systems, where this letter tends to draw attention to the quality factor and the phase information of the resonance modes, which indicates the damping characteristic of the system but was left out in the conventional modal analysis. In the studied cases, the current control interactions of VSCs, which are the power sources, are analyzed in a 3-bus test system. As the input admittance of the VSCs interacts with the passive components in the network, not only the magnitude-frequency responses of eigenvalues, but also their quality factors are required to analyze the resonance modes. Furthermore, the eigenvalues analyzed using the "circle fit" method show more insights than using the "peak-picking" method, where theoretical analysis is verified by case studies and experimental results.

II. Conventional Resonance Mode Analysis

In the conventional resonance mode analysis method [4], the relationship between voltages and currents has been described by the nodal admittance matrix, $[Y_f]$, at the given frequency, f, which is expressed as

$$[V_f] = [Y_f]^{-1}\,[I_f] \tag{1}$$

where $[V_f]$ represents the nodal voltage introduced by the nodal current injection $[I_f]$. Thus, the resonance occurs at the frequency when $[Y]$ approaches singularity. To investigate the singularity of $[Y]$, it can be diagonalized using the well-known eigenvalue analysis given as

$$[Y] = [L]\,[\Lambda]\,[T] \tag{2}$$

where $[L] = [T]^{-1}$. Then, the modal voltage vector, $[U] = [T]\,[V]$, and the modal current vector, $[J] = [T]\,[I]$ can be derived, and equation (1) can be simplified as

$$\begin{bmatrix} U_1 \\ U_2 \\ \vdots \\ U_N \end{bmatrix} = \begin{bmatrix} \lambda_1^{-1} & 0 & 0 & 0 \\ 0 & \lambda_2^{-1} & 0 & 0 \\ 0 & 0 & \ddots & 0 \\ 0 & 0 & 0 & \lambda_N^{-1} \end{bmatrix} \begin{bmatrix} J_1 \\ J_2 \\ \vdots \\ J_N \end{bmatrix} \tag{3}$$

where the inverse of the first eigenvalue, λ_1^{-1}, has been called the modal impedance of mode 1, $Z_{m,1}$, describing the relationship between U_1 and J_1. Since $[\Lambda]$ is a diagonal matrix, the other modal currents have no influence on U_1. Thus, in the studied frequency range, the smallest eigenvalue has been named the "critical resonance mode", which means a small modal current J can introduce a large modal voltage U. Following this concept, the study in [5] has concluded that attention should be paid to the magnitude of eigenvalues.

This article has been accepted for publication in a future issue of this journal, but has not been fully edited. Content may change prior to final publication. Citation information: DOI 10.1109/TPEL.2020.3032736, IEEE Transactions on Power Electronics

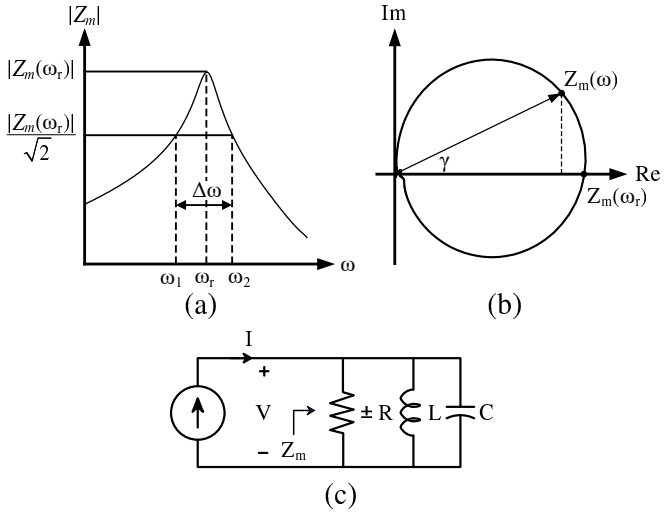

Fig. 1. Modal analysis with (a) Magnitude-frequency plot (b) Nyquist plot (c) Parallel RLC circuit.

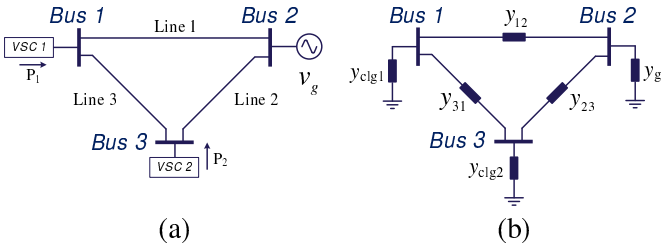

Fig. 2. (a) 3-bus test system configuration with two voltage source converters (b) The nodal admittance network representation.

III. Frequency-Domain Modal Analysis Methods

A. Peak-Picking Method

In essence, this analysis method is called the "peak-picking" method reported in [10], where in the studied frequency range, the resonance frequency ω_r is identified from the peak value of modal impedance as shown in Fig. 1 (a), and the half power points can be identified at each side of the peak with the value of $\frac{|Z_m|}{\sqrt{2}}$ at ω_1 and ω_2, where the bandwidth $\Delta\omega = \omega_2 - \omega_1$. Then, the quality factor, Q, can be estimated as

$$Q \approx \frac{\omega_r}{\Delta\omega} \tag{4}$$

where the system is underdamped with higher Q. Yet, Q is estimated by the half power points, which are only related to the peak eigenvalue $|Z_m(\omega_r)|$. The method is simple but might be affected by measurement errors [10].

B. Circle Fit Method

Alternatively, Z_m can be plotted in a Nyquist plot as the schematic diagram shown in Fig. 1 (b), which the method is called the "circle fit" method. The modal impedance Z_m is the linear combination of the admittances in (2), which may have multiple resonance frequencies. Yet, in the studied frequency range around a resonance frequency ω_r, the orthogonality of Z_m can be used to simplify the system as a second-order system [10], i.e. a parallel RLC circuit shown in Fig. 1 (c). Thus, Z_m can be derived as

$$Z_m = \frac{V}{I} = \frac{1}{C}\frac{s}{s^2 + \frac{1}{RC}s + \frac{1}{LC}} = \frac{1}{C}\frac{s}{s^2 + 2\alpha s + \omega_r^2} \tag{5}$$

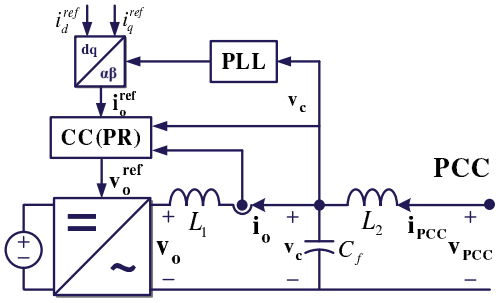

Fig. 3. VSC circuit diagram with its control system.

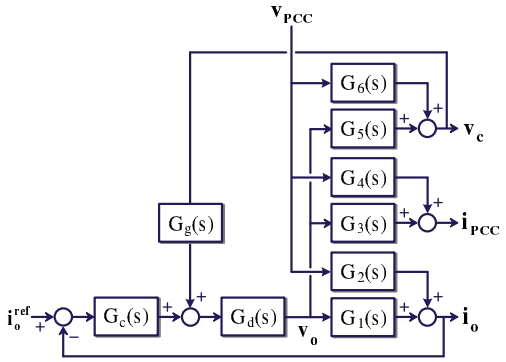

Fig. 4. Control block diagram.

where Q is equal to $\omega_r/2\alpha$, and it can be changed by the different values of R without changing the resonance frequency, ω_r. Therefore, the value of $|Z_m(\omega_r)|$ may also be influenced by Q. Then, by replacing s with $j\omega$, the ratio of the imaginary part to the real part of Z_m, which is also $\tan\gamma$, can be derived as

$$\tan\gamma = \frac{\mathrm{Im}(Z_m)}{\mathrm{Re}(Z_m)} = \frac{\omega_r^2 - \omega^2}{2\alpha\omega} \tag{6}$$

where the unknown variables, i.e. α and ω_r^2, can be solved by arbitrarily choosing two points on the plot shown in Fig. 1 (b). It is worth mentioning that the estimated Q in (4) is always positive. However, as the input admittances of VSCs have a negative-resistance characteristic in a wide frequency range, i.e. $-R$ in Fig. 1 (c), the Q with negative value can only be derived from (6). Note that negative Q factor generally exists in the system containing active components, e.g. current amplifier [11], where the VSCs serve as the active device in the power system. Furthermore, the negative Q in (6) indicates the existence of right half plane poles in Z_m, which Z_m is also the closed loop gain from J to U as shown in (3).

IV. Nodal Admittance Matrix Considering VSCs' Input Admittances

Fig. 2 (a) illustrates a 3-bus test system composed by two grid-connected VSCs. The transmission lines between buses are named as Line 1, Line 2, and Line 3, where VSC 1 and VSC 2 are connected at Bus 1 and Bus 3, respectively. Then, the circuit diagram and the control system of the individual VSC are shown in Fig. 3. Since the current control loop is of concern in this work, where the dc sides of VSCs are connected to ideal dc voltage sources to eliminate the influence of dc bus control dynamics, and the VSC connected to the point of common coupling (PCC) through an LCL-filter. The

filter capacitor voltage, $\mathbf{v_c}$, and converter side current, $\mathbf{i_o}$ are measured for the current controller (CC), which uses the proportional-resonant (PR) controller to regulate i_o in the $\alpha\beta$-frame. Then, the angle, θ, derived from the phase-locked loop (PLL) and the dq- to $\alpha\beta$-frame transformation are used to generate the current commands in the $\alpha\beta$-frame, $\mathbf{i_o^{ref}}$, from i_d^{ref} and i_q^{ref}. By setting the bandwidth of the PLL low and assuming $v_o = v_o^{ref}$ to neglect the frequency-coupling dynamics of PLL [2] and the non-linearity of pulse-width modulation, the control block diagram is then as illustrated in Fig. 4, where the blocks from $G_1(s)$ to $G_6(s)$ represent the open-loop transfer functions from $\mathbf{v_{PCC}}$ and $\mathbf{v_o}$ to $\mathbf{v_c}$, $\mathbf{i_o}$, and $\mathbf{i_{PCC}}$, respectively [12]. For the remaining blocks, $G_c(s)$ and $G_g(s)$ represent the CC and capacitor voltage feedforward controller, where $G_d(s)$ describes the total system time delay, and their forms are given as

$$G_c(s) = K_p + \frac{2K_r s}{s^2 + \omega_1^2} \qquad G_g(s) = 1$$
$$G_d(s) = e^{-1.5T_s s} \tag{7}$$

where T_s represents the sampling period, and $\omega_1 = 2\pi f_1$, where f_1 is the fundamental frequency. To simplify the notation, the "s" operator is omitted in the following transfer functions. Thus, the input admittance of the VSC can be derived as the ratio of $\mathbf{i_{PCC}}$ to $\mathbf{v_{PCC}}$ and given as

$$y_{clg} = \frac{\mathbf{i_{PCC}}}{\mathbf{v_{PCC}}} = G_4 + \frac{G_3G_6G_gG_d - G_2G_3G_cG_d}{1 + G_1G_cG_d - G_5G_gG_d} \tag{8}$$

where the s-domain expression in (8) is only used for the theoretical analysis purpose, which may not be derived in the frequency scan analysis. Since the VSC can be modeled as a current source in parallel with the admittance y_{clg} [9], the network in Fig. 2 (a) can then be illustrated as Fig. 2 (b), where the transmission lines are modeled as admittances, y_{12}, y_{23}, and y_{31}. Furthermore, considering the actual voltage source in Fig. 2 (a), the admittance y_g is included to represent the grid impedance. Thus, the nodal admittance matrix can be derived as

$$[Y] = \begin{bmatrix} y_{clg1} + y_{12} + y_{31} & -y_{12} & -y_{31} \\ -y_{12} & y_g + y_{12} + y_{23} & -y_{23} \\ -y_{31} & -y_{23} & y_{clg2} + y_{23} + y_{31} \end{bmatrix} \tag{9}$$

where it indicates that the input admittance of VSCs may also affect the analysis result when performing frequency scan analysis on a network containing VSCs, and the negative-resistance characteristic is then introduced to the nodal admittance matrix by y_{clg1} and y_{clg2}, where the matrix is used for modal analysis with case studies.

V. Case Studies and Experimental Verification

To reveal the influence of the Q factor in the modal analysis, different cases based on the system diagram in Fig. 2 (a) are tested in this section using the frequency-domain modal analysis and experimental verifications, where the system parameters used are listed in Table I, and the impedances of lines 1, 2 and 3 are considered as ideal components in the theoretical analysis.

TABLE I. Parameters used in experiment and case studies.

Symbol	Parameter Description	Value
v_g	Grid voltage	400 V_{rms}
P_1,P_2	Output power of VSCs	3.5 kW
f_1	Fundamental frequency	50 Hz
T_s	Sampling period	100 µs
L_1	Converter side inductor	3 mH
L_2	Grid side inductor	1 mH
$C_{f,1}$	Filter capacitor of VSC 1	10 µF
$C_{f,2}$	Filter capacitor of VSC 2	15 µF
y_{12}	Impedance of line 1	1 mH
y_{23}	Impedance of line 2	4 mH
y_{31}	Impedance of line 3	2 mH
y_g	Grid impedance	1.5 mH
K_r	Resonant gain in CC	1000 Ω/s
$K_{p,1}$	Proportional gain in CC of VSC 1	23.5 Ω 25 Ω 28 Ω
$K_{p,2}$	Proportional gain in CC of VSC 2	15.5 Ω

A. Peak-Picking Method

First, the system is tested with $K_{p,1} = 23.5\ \Omega$, the bus voltages are measured and shown in Fig. 5. Then, the spectrum of $V_{Bus,1}$ is derived by applying the fast Fourier transform to the voltage waveform in the Channel 1 of Fig. 5 illustrated in Fig. 6. With the system parameters in Table I, modal impedances, Z_m, are plotted with magnitude-frequency responses in Fig. 7 (a), where three resonant modes can be identified by $Z_{m,1}$, $Z_{m,2}$, and $Z_{m,3}$, but only $Z_{m,1}$ and $Z_{m,2}$ are discussed in the following part. The Q factors are estimated using the method specified in section III-A as 12.8 for $Z_{m,1}$ at 2050 Hz and 8.1 for $Z_{m,2}$ at 440 Hz. However, even though the Q factor at 2050 Hz is larger than the one at 440 Hz, the largest harmonic voltage is observed at 440 Hz like shown in Fig. 6 since $|Z_{m,2}|$ at 440 Hz is much higher than $|Z_{m,1}|$ at 2050 Hz. Then, when $K_{p,1}$ is increased to 25 Ω, the bus voltages are shown in Fig. 8, where $|Z_m|$ is plotted in Fig. 10 (a). The Q factor of $Z_{m,1}$ increases to 34.3. In this case, even if $|Z_{m,2}|$ at 450 Hz is still higher than $|Z_{m,1}|$ at 2055 Hz. The magnitude of harmonic voltage at 2055 Hz reaches the one caused by $Z_{m,2}$ at 450 Hz, which shows the influence of the Q factor to the resonance. To further investigate these resonance modes, $K_{p,1}$ is increased to 28 Ω, where the waveform shown in Fig. 11 is saved before the VSC is tripped, and the resonance becomes noticeable in $V_{Bus,1}$, and the largest resonance voltage occurs at 2070 Hz as shown in Fig. 12. However, the magnitude of the modal impedance $Z_{m,1}$ plotted in Fig. 13 (a) is not the largest one, and the Q factor estimated with magnitude-frequency plot with a value of 28.1 is even lower than the one in Fig. 10 (a), which is because the "peak-picking" method with magnitude-frequency response ignores the phase information and leads to a wrong estimation.

B. Circle Fit Method

With the method specified in section III-B, the resonance frequency ω_r and Q factor are derived in Fig. 7 (b) and Fig. 10 (b) for the cases of $K_{p,1} = 23.5\ \Omega$ and $K_{p,1} =$

This article has been accepted for publication in a future issue of this journal, but has not been fully edited. Content may change prior to final publication. Citation information: DOI 10.1109/TPEL.2020.3032736, IEEE Transactions on Power Electronics

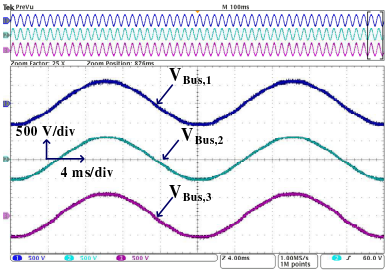

Fig. 5. Experimental waveforms of bus voltages in Fig. 2 with $K_{p,1} = 23.5\,\Omega$.

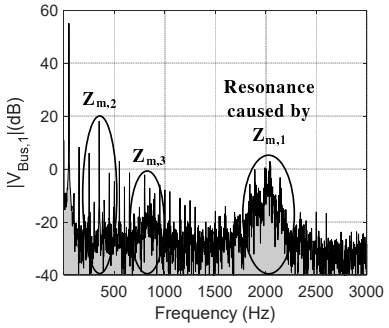

Fig. 6. FFT spectrum of $V_{Bus,1}$ in Fig. 5.

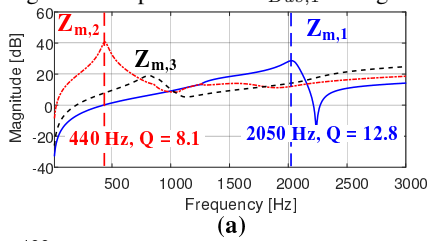

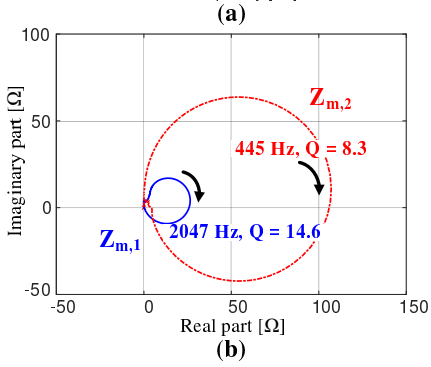

Fig. 7. Modal impedances, Z_m, of the case in Fig. 5 (a) Magnitude-frequency plot (b) Nyquist plot.

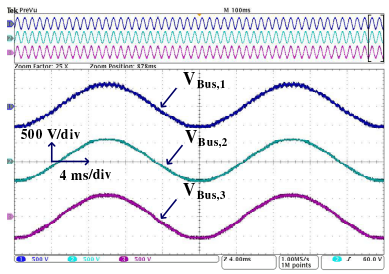

Fig. 8. Experimental waveforms of bus voltages in Fig. 2 with $K_{p,1} = 25\,\Omega$.

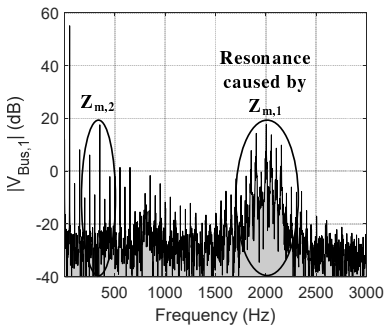

Fig. 9. FFT spectrum of $V_{Bus,1}$ in Fig. 8.

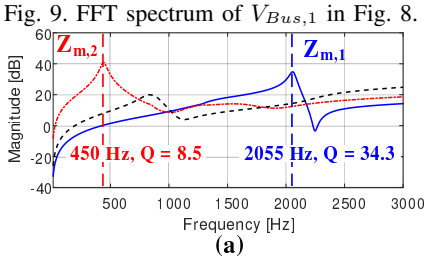

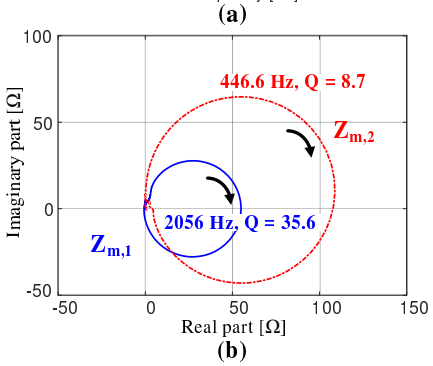

Fig. 10. Modal impedances, Z_m, of the case in Fig. 8 (a) Magnitude-frequency plot (b) Nyquist plot.

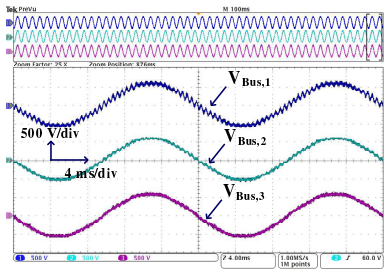

Fig. 11. Experimental waveforms of bus voltages in Fig. 2 with $K_{p,1} = 28\,\Omega$ before VSC tripped.

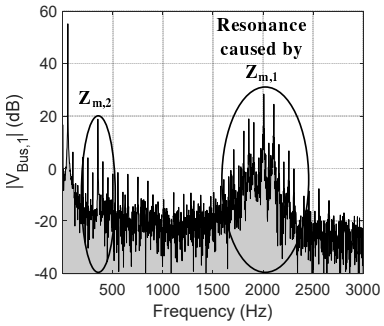

Fig. 12. FFT spectrum of $V_{Bus,1}$ in Fig. 11.

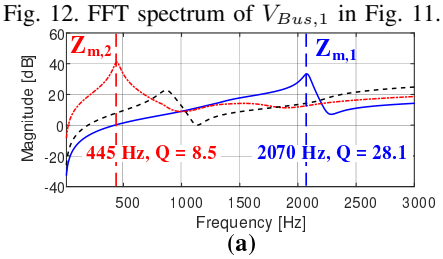

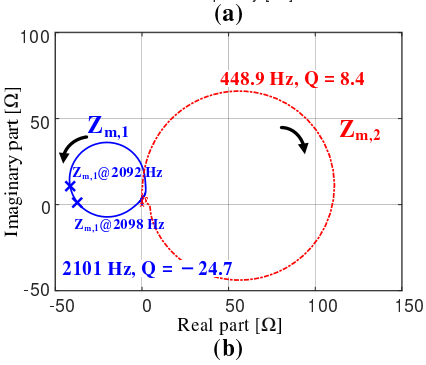

Fig. 13. Modal impedances, Z_m, of the case in Fig. 11 (a) Magnitude-frequency plot (b) Nyquist plot.

25 Ω, respectively. The numerically calculated values of ω_r and Q show more accurate results compared with the values estimated in section V-A, where the Nyquist plots with clockwise direction lead to positive Q. However, in Fig. 13 (b), two points, Z_{m1}@2092Hz $= -40.86 + 7.94j\Omega$ and Z_{m1}@2095Hz $= -37.89 + 2j\Omega$, are used to calculate the ω_r and Q with equation (6). The negative Q factor with value -24.7 is then numerically derived with counterclockwise Nyquist plot, which cannot be estimated in section V-A. Therefore, the phase information should also be investigated for assessing the singularity in the power electronic based power systems.

VI. Conclusions

In this letter, the 3-bus test system with VSCs as power sources is analyzed applying the frequency-domain modal analysis considering the input admittance of VSCs in the nodal admittance network to derive the modal impedances. To analyze the mode shape, two things should be considered: 1) The Q factor is as important as the magnitude of modal impedance in modal analysis. 2) The negative value of the Q factor depicts that the studied system is active, where the Nyquist plot can be used to numerically calculate the resonance frequency and Q factor. The case studies and experimental results validate the theoretical modal analysis.

REFERENCES

[1] F. Blaabjerg, Y. Yang, D. Yang, and X. Wang, "Distributed power-generation systems and protection," *Proceedings of the IEEE*, vol. 105, no. 7, pp. 1311–1331, July 2017.

[2] X. Wang, F. Blaabjerg, and W. Wu, "Modeling and analysis of harmonic stability in an ac power-electronic-based power system," *IEEE Trans. Power Electron.*, vol. 29, no. 12, pp. 6421–6432, Dec. 2014.

[3] S.-F. Chou, X. Wang, and F. Blaabjerg, "Reflection Coefficient Stability Criterion for Multi-Bus Multi-VSC Power Systems," *IEEE Access*, vol. 8, pp. 111 186–111 199, 2020.

[4] W. Xu, Z. Huang, Y. Cui, and H. Wang, "Harmonic Resonance Mode Analysis," *IEEE Trans. Power Del.*, vol. 20, no. 2, pp. 1182–1190, April 2005.

[5] Z. Huang, Y. Cui, and W. Xu, "Application of Modal Sensitivity for Power System Harmonic Resonance Analysis," *IEEE Trans. Power Syst.*, vol. 22, no. 1, pp. 222–231, Feb 2007.

[6] H. Hu, H. Tao, X. Wang, F. Blaabjerg, Z. He, and S. Gao, "Train–Network Interactions and Stability Evaluation in High-Speed Railways—Part II: Influential Factors and Verifications," *IEEE Transactions on Power Electronics*, vol. 33, no. 6, pp. 4643–4659, 2018.

[7] L. Hong, W. Shu, J. Wang, and R. Mian, "Harmonic Resonance Investigation of a Multi-Inverter Grid-Connected System Using Resonance Modal Analysis," *IEEE Transactions on Power Delivery*, vol. 34, no. 1, pp. 63–72, 2019.

[8] Z. Liu, J. Rong, G. Zhao, and Y. Luo, "Harmonic Assessment for Wind Parks Based on Sensitivity Analysis," *IEEE Transactions on Sustainable Energy*, vol. 8, no. 4, pp. 1373–1382, 2017.

[9] X. Wang and F. Blaabjerg, "Harmonic Stability in Power Electronic Based Power Systems: Concept, Modeling, and Analysis," *IEEE Trans. Smart Grid*, vol. 10, no. 3, pp. 2858–2870, May 2019.

[10] J. He and Z.-F. Fu, *Modal Analysis*. Butterworth-Heinemann, 2001. [Online]. Available: http://www.sciencedirect.com/science/article/pii/B9780750650793500000

[11] K. Koli, "CMOS Current Amplifiers: Speed versus Nonlinearity," Ph.D. dissertation, chapter 6, Helsinki University of Technology Electronic Circuit Design Laboratory, 2000.

[12] S.-F. Chou, X. Wang, and F. Blaabjerg, "Passivity-based LCL Filter Design of Grid-Connected VSCs with Converter Side Current Feedback," in *2018 International Power Electronics Conference (IPEC-Niigata 2018 -ECCE Asia)*, 2018, pp. 1711–1718.